J. Fluid Mech. (2004), *vol.* 506, *pp.* 331–355.
DOI: 10.1017/S0022112004008638 Printed in the United Kingdom

Self-similar solutions of the axisymmetric shallow-water equations governing converging inviscid gravity currents

By ANJA C. SLIM AND HERBERT E. HUPPERT

Institute of Theoretical Geophysics, Department of Applied Mathematics and Theoretical Physics, Centre for Mathematical Sciences, University of Cambridge, Wilberforce Road, Cambridge, CB3 0WA, UK

(Received 2 August 2003 and in revised form 5 January 2004)

A phase-plane approach is used to determine similarity solutions of the axisymmetric shallow-water equations which represent inwardly propagating, inviscid gravity currents. A Froude number condition characterizes the movement of the front. The unique similarity exponent is found numerically as a function of the frontal Froude number and the height and velocity profiles are presented for three different Froude numbers. The fluid speed and height are seen to increase monotonically towards the front except very close to the front where the height decreases. The maxima in both height and speed increase as the Froude number increases, reflecting the change in ambient resistance.

For the Froude number that has been obtained experimentally for lock-exchange Boussinesq flows ($Fr = 1.19$) for which the similarity exponent is 0.859094, the similarity solution is compared to the numerical solution of the initial value problem, obtained recently by Hallworth, Huppert & Ungarish (2003). Our similarity solution compares reasonably well with their integration of the shallow-water equations in the neighbourhood of the front and at times close to collapse (when the front reaches the origin); however, near this point their numerics begin to fail. The solution at collapse and the similarity solution after collapse are also found for $Fr = 1.19$. This similarity solution describes the formation of a shock, as well as its initial propagation.

1. Introduction

There are many examples of gravity currents in nature, such as fog banks, river water discharging into the sea and pyroclastic flows. They occur whenever fluid of one density flows, predominantly horizontally, into fluid of a different density. The density contrasts that drive the current may be due to differences in temperature or composition. An overall view of many of the phenomena associated with gravity currents is presented by Simpson (1997).

The situation which we consider here is that of a converging, axisymmetric gravity current propagating at high Reynolds number. An example of such a flow in nature is where turbidity currents are generated at the edge of a lake and propagate inwards towards the lake's centre. Another example is tidal flow up a river estuary, although this is not strictly axisymmetric due to bank friction and an irregular geometry. The funnelling effect of the estuary greatly enhances tidal variation, and estuaries such as that of the Severn are great (potential) sources of tidal power.

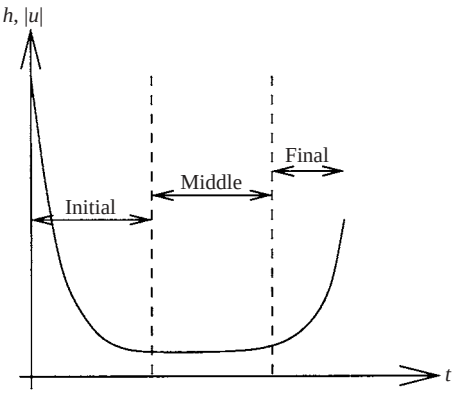

FIGURE 1. Qualitative structure of the height and velocity of the current front against time. 'Initial' refers to the behaviour at early times during which the height of the front reduces with time. 'Middle' refers to intermediate times during which the height of the front is fairly constant with time. 'Final' refers to late times, just before collapse, during which the height of the front increases once more. Redrawn from Hallworth *et al.* (2003).

The precise flow which we consider is the axisymmetric gravity current that results when fluid contained between two concentric circular cylinders is suddenly released by the removal of the inner cylinder. This problem was considered in an experimental and numerical framework by Hallworth, Huppert & Ungarish (2003). They found that the gravity current produced passes through three phases before the front reaches the origin (the axis of the cylinders), as shown in figure 1. Initially, the inwardly propagating current develops in a way similar to an outflowing current, with the height and the velocity of the front decreasing with time (or increasing distance from the lock). However, the narrowing of the geometry causes fluid to pile up at the front and eventually this effect becomes comparable to the lowering of the front due to spreading of the current. Therefore the next stage is typified by fairly constant height and velocity of the front. In the final stage, when the front is very close to the origin, its height and velocity increase. We present a similarity solution for this final stage. In order to do so, we model the current using the shallow-water equations. These are appropriate equations for shallow inviscid currents and are the same as those used in Hallworth *et al.* (2003).

There are several reasons for considering similarity solutions. First, they describe the intermediate asymptotics of a problem: they hold at times when the precise initial conditions are no longer important, but before the system has reached its final steady state. They are also much simpler than the full solutions and so should be easier to understand and study in different regions of parameter space. A final reason for studying them is that they are solutions of a system of ordinary differential equations and hence do not suffer the extra inherent numerical problems of the full partial differential equations, in this case the hyperbolic shallow-water equations.

In the regime in which we are interested, both the radius of the outer cylinder and the total volume of fluid are likely to be important at all times (we describe this in more detail in § 3). This suggests that any similarity solution is not of the standard form but is of the second kind (Barenblatt 1996). In order to find it, we use the powerful phase-plane approach in which the system is assumed to be self-similar, but with an unknown similarity exponent. This reduces the governing partial differential equations to a set of autonomous ordinary differential equations in two variables and

the boundary conditions to points in their phase space. The problem then reduces to finding the similarity exponent for which an integral curve connects the points representing the boundary conditions. This is also explained in greater detail in § 3. The approach has been used extensively in gas dynamics to find similarity solutions (see, for example, Sedov 1959; Barenblatt 1996). In particular, the problem analogous to ours, that of an imploding axisymmetric shock, has been considered in detail using this method by many authors, such as Guderley (1942), Brushlinskii & Kazhdan (1963) and Bilbao & Gratton (1996). It has also been used in many other fields, for example, Gratton & Minotti (1990) used it to study self-similar viscous gravity currents including converging currents, while Aronson & Graveleau (1993) and Diez, Gratton & Minotti (1992*a*) applied the method to find inwardly propagating solutions of more general diffusion-type equations. The problem of converging, surfactant-driven flow was considered by Jensen (1994); Hunter (1960) modelled cavitation and Grigoryan & Babkin (1998) studied turbulent converging currents. The phase-plane approach has also been used in the study of the shallow-water equations by Grundy & Rottman (1986). They discussed similarity solutions to both the planar and axisymmetric problem of an outflowing current with time-dependent flux at the origin. Their work was considerably extended by Gratton & Vigo (1994) in the planar case to incorporate shocks.

The layout of the paper is as follows. In § 2 we set up the shallow-water equations and boundary conditions for our problem and in § 3 translate them into the phase-plane formalism. In § 3.7 we find the similarity solution and study how it changes with changing frontal Froude number. In § 4 we compare our similarity solution to the behaviour of the initial value problem at times when the front is close to the origin. We investigate the comparison with the results of numerical integration of the shallow-water equations, using the numerical code of Hallworth *et al.* (2003). A comparison with their experimental results is not possible since too few measurements exist of the final stages of the flow, just before collapse. In § 5 we briefly consider the solution when the front reaches the origin and the similarity solution thereafter. In § 6 we summarize the main features of the similarity solutions we have found and discuss their accuracy in modelling the physical problem.

2. Formulation of the problem

We consider an axisymmetric gravity current whose front propagates inwards, towards the origin. Such a current results when fluid contained between two concentric circular cylinders is suddenly released due to the removal of the inner cylinder. We are interested in the cases when the current is either more or less dense than the ambient fluid into which it is intruding. If the current is more dense, then it flows over a lower boundary. If it is less dense, then it flows under an upper boundary. In either case the bounding surface is taken to be flat and horizontal.

2.1. *Assumptions and governing equations*

We assume that the ambient fluid has a depth much greater than the height of the current and that both the ambient and the current have homogeneous densities. We ignore any flow in the ambient and also mixing, surface tension and frictional effects between the current and the ambient, except at the front (see § 2.2).

We consider the regime in which inertia and buoyancy balance and viscosity and turbulence are negligible. At sufficiently long times after release, the current's length

may be taken to be much greater than its thickness and the flow in the current may be taken to be predominantly horizontal. Hence pressure may be assumed hydrostatic.

Under these assumptions, the appropriate governing equations for the gravity current are the axisymmetric shallow-water equations

$$\frac{\partial h}{\partial t} + \frac{1}{r}\frac{\partial}{\partial r}(ruh) = 0, \tag{2.1a}$$

$$\frac{\partial u}{\partial t} + u\frac{\partial u}{\partial r} + g'\frac{\partial h}{\partial r} = 0, \tag{2.1b}$$

which can be obtained from the depth-integrated mass and momentum equations (see, for example, Penney & Thornhill 1952; Whitham 1974). In these equations, u is the radial velocity, h height, t time and r the radial coordinate. The parameter g' is the reduced gravity, given by $g' = (\rho - \rho_a)g/\rho$, where ρ_a is the density of the ambient and ρ that of the current. It should be noted that we are not taking the Boussinesq approximation here because we are interested in all possible ratios of densities between the current and the ambient, although taking the Boussinesq approximation would not change the form of the equations.

2.2. *Boundary conditions*

During the motion, the outer cylinder at $r = R_o$ remains in place and the velocity there is zero. Hence one boundary condition for (2.1) is

$$u(R_o, t) = 0. \tag{2.2}$$

The boundary condition at the front must describe the influence of the ambient fluid on the gravity current. This has been neglected so far in our formalism, other than replacing g with g' in the shallow-water equations (2.1). Most work on finding such a front condition has been done for the planar lock-exchange problem and to motivate our choice we give a brief description of the relevant results for that situation.

At the front, there is a quasi-steady balance between the current's buoyancy, driving it inwards, and the acceleration of the ambient as it is forced to rise over the current if it is less dense or to sink under the current if it is more dense. There is then a relation between the velocity and height of the front given by

$$\frac{u(r_f, t)}{\sqrt{g'h(r_f, t)}} = Fr, \tag{2.3a}$$

where Fr is the frontal Froude number and r_f is the position of the front and satisfies

$$\frac{\mathrm{d}r_f}{\mathrm{d}t} = u(r_f, t). \tag{2.3b}$$

Such a relation was first derived by von Kármán (1940) and Benjamin (1968) and has been used extensively in subsequent work on inviscid gravity currents (see Huppert 2000). It should be noted that the height and velocity here are not those at the point where the height of the current is zero, but the constant values just behind the head of the current.

The value of the frontal Froude number in (2.3) depends on the density contrast between the current and the ambient. Benjamin (1968) used conservation of mass and momentum to obtain the Froude number for a current of zero density propagating into an ambient of non-zero density with energy loss. His result was extended by Gröbelbauer, Fanneløp & Britter (1993) to currents of non-zero density and they

derived

$$Fr = \sqrt{2\rho/\rho_a}, \tag{2.4}$$

for an infinite ambient. However, they modified this relation so that in the limit $\rho/\rho_a \to \infty$, $Fr \to 2\sqrt{2}$ based on the finite rate of exchange of energy in the current from potential to kinetic. They also conducted a numerical and experimental investigation, with the results agreeing reasonably well with (2.4).

More recently, Shin, Dalziel & Linden (2004) have argued that energy is conserved in a planar lock-exchange system, although it is transported between the heavy and light fluid fronts. Using conservation of mass, momentum and energy, as well as the unsteady Bernoulli equation, they obtain

$$Fr = 1, \tag{2.5}$$

for an infinite ambient and for Boussinesq fluids. For this case, Huppert & Simpson (1980) experimentally obtained the relation

$$Fr = 1.19, \tag{2.6}$$

for the heavy fluid front.

While these results are not rigorously applicable, particularly since the flow in our current is not steady as assumed in the theoretical derivations given above, we use them as a guide. Hence we take our frontal condition to be identical to (2.3), although in view of the fact that $u < 0$ we write

$$\frac{u(r_f, t)}{\sqrt{g'h(r_f, t)}} = -Fr, \tag{2.7a}$$

$$\frac{\mathrm{d}r_f}{\mathrm{d}t} = u(r_f, t). \tag{2.7b}$$

From (2.4), we take the Froude number to be a constant in the range 0 to infinity, with large (small) values corresponding to large (small) current densities compared to the ambient. We ignore the fact that (2.3) does not hold precisely at the front, but just behind the head.

2.3. *Jump conditions*

Internal jumps may occur at the interface between the current and the ambient fluid and we should consider this possibility in our similarity solution. They turn out to be of interest in finding a similarity solution before collapse and are essential to our analysis of behaviour after collapse (see § 5) and so we give a brief description of them here. Because the depth of the ambient has been taken to be infinite, the conditions governing any internal jumps are identical to those for a single-layer fluid (see Yih & Guha 1955) and may be obtained from conservation of mass and momentum across the shock. If u_s is the velocity of the shock and r_s its radial position, then

$$\frac{\mathrm{d}r_s}{\mathrm{d}t} = u_s, \tag{2.8a}$$

$$u' - u_s = 2(u - u_s)/\phi(Fr_s), \tag{2.8b}$$

$$h' = \tfrac{1}{2}h\phi(Fr_s), \tag{2.8c}$$

where $\phi(Fr_s) = (1 + 8Fr_s^2)^{1/2} - 1$ and $Fr_s = (u - u_s)/\sqrt{g'h}$. Here unprimed variables refer to values behind the shock and primed variables to values ahead of the shock (see Yih & Guha 1955; Gratton 1991).

Using a Kármán–Pohlhausen technique, it may also be possible to derive an alternative set of governing equations which include shocks automatically (see Watanabe, Putkaradze & Bohr 2003). We have not considered that approach, although it may be interesting to do so.

3. Self-similarity

In this section we consider the problem of finding a similarity solution of the shallow-water equations (2.1) subject to the boundary conditions of § 2.2. As an introduction and indication of the notation, we summarize the theory behind self-similarity, with our formal analysis beginning in § 3.1.

First we non-dimensionalize the problem. The shallow-water equations can be reduced to a pair of equations with no dependence on constant parameters if, instead of considering the variable h, we consider the variable $\hbar = g'h$. Then the variables and parameters for our problem, with their dimensions, are

u	$\hbar$	r	t	$g'V$	R_o	Fr	a_1	a_2	$\ldots$
LT^{-1}	L^2T^{-2}	L	T	L^4T^{-2}	L	1	1	1	$\ldots$

where V is the volume of the current, R_o is the radius of the outer cylinder and a_1, a_2, ... are dimensionless parameters which characterize the precise initial conditions. It should be noted that all the parameters are kinematic and hence only two may have independent dimensions.

The dimensionless variables are then

$$\frac{u}{r/t} \qquad \frac{\hbar}{r^2/t^2} \qquad \underbrace{\frac{r}{(g'V)^{1/4}|t|^{1/2}}}_{\xi_1} \qquad \underbrace{\frac{r}{R_o}}_{\xi_2} \qquad Fr \qquad a_1 \qquad a_2 \qquad \ldots$$

and so the dependent variables $u/(r/t)$ and $\hbar/(r^2/t^2)$ must satisfy

$$\frac{u}{r/t} = F_1(\xi_1, \xi_2, Fr, a_1, a_2, \ldots), \tag{3.1a}$$

$$\frac{\hbar}{r^2/t^2} = F_2(\xi_1, \xi_2, Fr, a_1, a_2, \ldots). \tag{3.1b}$$

The definition of self-similarity, given by Barenblatt (1996), is that 'a phenomenon is called self-similar if the spatial distribution of its properties at various moments of time can be obtained from one another by a similarity transformation'. The forms given in (3.1) are not self-similar because Barenblatt's definition requires that both r and t are tied together in a single dimensionless variable.

Shortly after the flow is initiated, we expect that a similarity solution will not hold, because both the volume of the current (multiplied by g') and the radius of the outer cylinder, in addition to the precise form of the initial conditions, will be important. For a similarity solution to hold at later times, the system must forget either $g'V$ or R_o, or a single number representing both must be selected. For it to be useful, the system should also forget the initial conditions.

If we set the moment of collapse to be $t = 0$, then we seek the similarity solution valid in the limit as $t \to 0^-$. In this limit, there are three possibilities for the behaviour of (3.1). These are:

(*a*) self-similarity of the first kind, where

$$F_i(\xi_1, \xi_2, Fr, a_1, a_2, \ldots) \to \tilde{F}_i(\xi_1, Fr, a_1, a_2, \ldots) \quad \text{or} \quad \tilde{F}_i(\xi_2, Fr, a_1, a_2, \ldots)$$

for $i = 1, 2$;

(*b*) self-similarity of the second kind, where

$$F_i(\xi_1, \xi_2, Fr, a_1, a_2, \dots) \to \tilde{F}_i\left(\xi_1/\xi_2^{\alpha}, Fr, a_1, a_2, \dots\right)$$

for $i = 1, 2$ and for specific α; and

(*c*) no limit for $F_{1,2}$ exists of the above forms. Self-similarity may then not exist. Further details of this argument are given by Barenblatt (1996).

Hence for similarity solutions of both the first and second kind, the form of the solutions for the dependent variables can be written as

$$\frac{u}{r/t} = \tilde{F}_1(\eta), \quad \frac{\hbar}{r^2/t^2} = \tilde{F}_2(\eta), \tag{3.2}$$

where $\eta = r/b|t|^{\delta}$ and is dimensionless. For similarity solutions of the first kind, only a single boundary condition is still important in the regime of interest and hence b and δ are fixed by it. For similarity solutions of the second kind, this is no longer the case and b and δ are not fixed by a single boundary condition. This is expected to be the case for our problem, since a major factor affecting our similarity solution will be the volume of fluid concentrated in the head of the current, because this controls the height and hence dynamics of the front. This is clearly related to the total volume of fluid (multiplied by g'); however, it is also related to the radius of the outer cylinder since the current will wet the entire area from the outer cylinder to the front at all times. For such similarity solutions, δ is found by solving an eigenvalue problem: for general δ no solution exists and only for a specific value of δ is a solution possible. The value of δ also sets the dimensions of b. However, the numerical value of b can only be found by following an initial value problem, either numerically or experimentally, until it reaches the self-similar regime (see Barenblatt 1996).

It turns out to be convenient to scale $\tilde{F}_1$ and $\tilde{F}_2$ with δ and δ^2 respectively (in the analysis later, this keeps important features in the phase plane fixed with changing δ). Then the final forms that we assume for η and for the dependent variables u and $\hbar$ are

$$u = \delta\frac{r}{t}v(\eta), \quad \hbar = \delta^2\frac{r^2}{t^2}z(\eta), \quad \eta = \frac{r}{b|t|^{\delta}}, \tag{3.3}$$

where v and z are dimensionless functions of η. It should be noted that before collapse $t < 0$ and for an inwardly propagating current $u < 0$, and therefore $v > 0$. The position of the front, r_f, is given by $r_f = b|t|^{\delta}$.

3.1. *Phase-plane governing equations*

Substituting (3.3) into the shallow-water equations (2.1), we obtain, after considerable algebra,

$$\frac{\mathrm{d}v}{\mathrm{d}\log\eta} = \frac{v(1-v)(1-\delta v) + 2z(1-\delta-\delta v)}{\delta[z-(v-1)^2]}, \tag{3.4a}$$

$$\frac{\mathrm{d}z}{\mathrm{d}\log\eta} = \frac{z(3\delta v^2 - 4\delta v - v + 2 - 2\delta z)}{\delta[z-(v-1)^2]}. \tag{3.4b}$$

These equations should be compared to those derived when studying self-similarity in gas dynamics, since much work has been done in that field. The axisymmetric governing equations for an ideal, inviscid, polytropic gas neglecting heat conduction

and body forces (Whitham 1974) are

$$\frac{\partial u_g}{\partial t} + u_g \frac{\partial u_g}{\partial r} + \frac{1}{\rho_g}\frac{\partial p_g}{\partial r} = 0, \tag{3.5a}$$

$$\frac{\partial \rho_g}{\partial t} + \frac{1}{r}\frac{\partial}{\partial r}(r\rho_g u_g) = 0, \tag{3.5b}$$

$$\frac{\mathrm{D}}{\mathrm{D}t}\left(p_g \rho_g^{-\gamma}\right) = 0, \tag{3.5c}$$

where u_g is the velocity, ρ_g the density, p_g the pressure of the gas and γ the adiabatic exponent. Note that these equations can be made identical to the shallow-water equations in the case $\gamma = 2$ on introducing the transformations $p_g = \rho g' h^2/2$, $\rho_g = \rho h$ and $u_g = u$.

Then substituting

$$u_g = \delta \frac{r}{t} v(\eta), \quad \rho_g = A_\omega G(\eta) r^{-\omega}, \quad \gamma \frac{p_g}{\rho_g} = \delta^2 \frac{r^2}{t^2} z(\eta), \tag{3.6}$$

where $\eta = r/b|t|^\delta$, into (3.5), we obtain identical equations to (3.4) for v and z if and only if $\gamma = 2$ and $\omega = 2(1-\delta)/\delta$ (see Gratton 1991). The problem in gas dynamics analogous to that with which we are dealing is an imploding cylindrical shock. This problem has been studied in some detail for $\omega = 0$ (an initially uniform density distribution) and ω a constant (Ferro Fontan, Gratton & Gratton 1977). However, to our knowledge, it has not been studied for ω a function of δ, in particular not for the special case $\omega = 2(1-\delta)/\delta$. The combination of different ω and different boundary and jump conditions in our problem results in different phase-plane and solution structures from those of gas dynamics.

3.2. *Phase-plane boundary conditions*

In the similarity variable η, the outer cylinder at $r = R_o$ has coordinate $\eta_o = R_o/b|t|^\delta$. Because we seek a similarity solution in the limit as $t \to 0^-$, the boundary condition of zero velocity at the outer cylinder (2.2) becomes

$$u \to 0 \begin{cases} \text{as } \eta \to \infty: & \delta > 0 \\ \text{as } \eta \to f: & \delta = 0 \\ \text{as } \eta \to 0: & \delta < 0, \end{cases} \tag{3.7}$$

where f has some finite, non-zero value.

To obtain the frontal boundary condition in (v, z) coordinates, we substitute (3.3) into (2.7) to yield

$$v_f = 1, \quad z_f = \frac{1}{Fr^2}, \tag{3.8}$$

and without loss of generality we can set $\eta_f = 1$.

3.3. *Phase-plane jump conditions*

In (v, z) coordinates, the jump conditions (2.8) become

$$v' - 1 = \frac{2}{\phi(Fr_s)}(v-1), \quad z' = \tfrac{1}{2} z \phi(Fr_s), \tag{3.9}$$

where $Fr_s = (v-1)/z^{1/2}$.

3.4. *Discussion of the phase plane*

The governing equations and boundary conditions have now been translated into similarity form and to find our solution we could obtain $\mathrm{d}v/\mathrm{d}z$ from (3.4) and integrate to give $v(z)$. Next, from $\mathrm{d}z/\mathrm{d}\log\eta$ we could integrate to obtain $z(\eta)$ and hence $v(\eta)$, subject to the boundary conditions (3.7) and (3.8). However, we do not proceed in this way for two reasons. First, we do not yet know which point in (v, z)-space corresponds to (3.7). Secondly, because we are dealing with a similarity solution of the second kind, δ is unknown in advance. Hence we need to study how the behaviour of solutions changes with changing δ.

Instead, we consider the (v, z) phase plane. Reparameterizing in terms of a variable λ, where

$$\frac{\mathrm{d}\log\eta}{\mathrm{d}\lambda} = \delta[z - (v-1)^2], \tag{3.10}$$

we see that equations (3.4) become

$$\frac{\mathrm{d}v}{\mathrm{d}\lambda} = v(1-v)(1-\delta v) + 2z(1-\delta-\delta v), \tag{3.11a}$$

$$\frac{\mathrm{d}z}{\mathrm{d}\lambda} = z(3\delta v^2 - 4\delta v - v + 2 - 2\delta z), \tag{3.11b}$$

a simpler system of two autonomous ordinary differential equations, without the singularities of (3.4).

An example of the (v, z) phase plane is given in figure 2 where the bold arrows indicate increasing λ. Any orbit, including any fixed point, or part of any orbit represents a similarity solution for some boundary conditions. In fact, a solution can consist of bits of multiple orbits provided that they match, via the jump conditions (3.9), at ends which are not fixed by boundary conditions. Any conceivable similarity solution of the shallow-water equations (2.1) of the form of (3.3) can be obtained from the phase plane.

3.5. *Investigation of the fixed points*

We first consider the problem of finding which point in the phase plane corresponds to (3.7). For $\delta = 0$ we need to look at points at which $u \to 0$ as $\eta \to f$, some finite, non-zero value. We deal with this special case in a separate section (§ 3.8). For $\delta \neq 0$, we need to consider points at which $u \to 0$ as $\log\eta \to \pm\infty$. A necessary (but not sufficient) condition for $\log\eta = \pm\infty$ is that $\lambda = \pm\infty$. This can be seen from (3.10) unless v or z become infinite for finite λ, in which case a similar analysis with $1/v$ or $1/z$ holds.

From standard theory on ordinary differential equations (see, for example, Glendinning 1994), any orbit can only start or end, and hence have $\lambda = \pm\infty$, at a fixed point, a periodic orbit or a heteroclinic cycle. However, for (3.11) it can be shown using Dulac's criterion and the position of the nullclines that no periodic orbit or heteroclinic cycle can lie entirely within the $z \geqslant 0$ half-plane. Then, as $z = 0$ is an orbit and hence no other orbits can cross it, we have the result that orbits can only start and end at fixed points in the $z \geqslant 0$ half-plane. Since physically $g'h$ must be non-negative, only the half-plane $z \geqslant 0$ is relevant.

From this analysis we see that $\log\eta$ can only be infinite at the fixed points. We must now analyse all the fixed points to find which (if any) correspond to (3.7).

The leading-order asymptotic behaviour of $v(\eta)$ and $z(\eta)$ at each fixed point in the finite plane can be found by expanding $\mathrm{d}v/\mathrm{d}z$ and $\mathrm{d}z/\mathrm{d}\log\eta$ about the fixed point

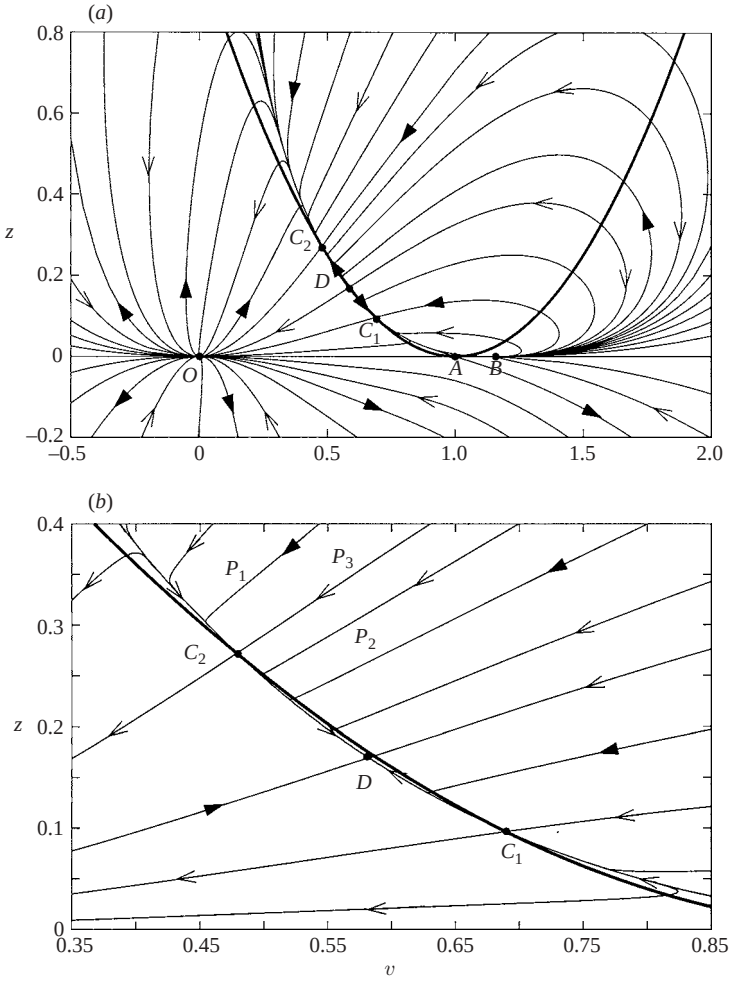

FIGURE 2. The (v, z) phase plane for $\delta = 0.859094$ (the similarity exponent for $Fr = 1.19$). Bold arrows indicate the direction of increasing λ and plain arrows indicate increasing η. The bold curve is the critical parabola $z = (v-1)^2$. Note that only A, C_1 and C_2 lie on this curve; D does not. (*a*) A global view of the phase plane and (*b*) a more detailed plot of the region around the fixed points C_1 and C_2. The curve P_3 is the minor-axis solution for the fixed point C_2 and the curves P_1 and P_2 show the abrupt change in direction of the integral curves close to C_2.

and integrating. Using the relations

$$u = \delta b |t|^{\delta} t^{-1} \eta v(\eta), \tag{3.12a}$$

$$\hbar = \delta^2 b^2 |t|^{2(\delta-1)} \eta^2 z(\eta), \tag{3.12b}$$

we can then obtain the values of u and $\hbar$. In addition, there are fixed points at which either or both of v and z are infinite. To consider the behaviour about these points we need to consider the equations involving the relevant reciprocals: either $1/v$ or $1/z$.

The leading-order behaviour and the limiting values of η, v, z, u, $\hbar$ and the flux $2\pi r u \hbar$ are given in tables 1 and 2 for $\delta \neq 0, 1$ and in table 3 for $\delta = 1$. From these

Fixed point	v	z	Type of fixed point in variable λ	$v(\eta)$	$z(\eta)$
O	0	0	UN	$K\eta^{-1/\delta}$ $2(1-\delta)K\eta^{-2/\delta}$ $K\eta^{-1/\delta}$	$\mathbf{0}$ $K\eta^{-2/\delta}$ $K'\eta^{-2/\delta}$
A	1	0	S	$1 \pm \left[2\frac{\delta-1}{\delta}(1+K\eta)\right]^{\frac{1}{2}}$ $\begin{cases} 1+\frac{2\delta-1}{\delta}(1+K\eta) & \delta \neq \frac{1}{2} \\ \mathbf{1} & \delta = \frac{1}{2} \end{cases}$	$\mathbf{0}$ $\begin{cases} \frac{\delta-1}{\delta}(1+K\eta) \\ \frac{1}{2}(\mathbf{1}+\boldsymbol{K\eta^{-2}}) \end{cases}$
B	$1/\delta$	0	SN for $\delta \notin (0,1)$ UN for $\delta \in (0,1)$	$\frac{1}{\delta}+K\eta^{1/(\delta-1)}$ $\frac{1}{\delta}+\frac{2\delta^2}{\delta-1}K\eta^{2/(\delta-1)}$ $\frac{1}{\delta}+K\eta^{1/(\delta-1)}$	$\mathbf{0}$ $K\eta^{2/(\delta-1)}$ $K'\eta^{2/(\delta-1)}$
C_1	v_1	z_1	UF for $\delta \notin (\delta_-^*, \delta_+^*)$ UN for $\delta \in (\delta_-^*, 0)$ SN for $\delta \in (0, \delta_-)$ SN for $\delta \in (\delta_+, 1)$ UN for $\delta \in (1, \delta_+^*)$	v_1 v_1	z_1 z_1
C_2	v_2	z_2	SF for $\delta \notin (\delta_-^*, \delta_+^*)$ SN for $\delta \in (\delta_-^*, \delta_-)$ SN for $\delta \in (\delta_+, \delta_+^*)$	v_2 v_2	z_2 z_2
D	$\frac{1}{2\delta}$	$\frac{1}{8\delta^2}$	S for $\delta \notin (\delta_-, \delta_+)$	$\frac{1}{2\delta}+\frac{1-\sqrt{64\delta^2-64\delta+17}}{2(2\delta-1)}\delta K\eta^{\alpha_-}$	$\frac{1}{8\delta^2}+K\eta^{\alpha_-}$
			SN for $\delta \in (\delta_-, \delta_+)$	$\frac{1}{2\delta}+\frac{1+\sqrt{64\delta^2-64\delta+17}}{2(2\delta-1)}\delta K\eta^{\alpha_+}$	$\frac{1}{8\delta^2}+K\eta^{\alpha_+}$
E	$\frac{1-\delta}{\delta}$	∞	S	$\frac{\mathbf{1-\delta}}{\boldsymbol{\delta}}+\boldsymbol{K\eta^{-2}}$ $\frac{1-\delta}{\delta}-\frac{(1-2\delta)(1-\delta)}{4\delta^2}K\eta^2$	∞ $\frac{1}{K}\eta^{-2}$
F	∞	0	S	∞ $K\eta^{-1}$	$\boldsymbol{K\eta^{-3}}$ $\mathbf{0}$
G	∞	∞	S–N	∞ $\frac{\mathbf{1-\delta}}{\boldsymbol{\delta}}+\boldsymbol{K\eta^{-2}}$ $K\eta^{-4/3}$	$\boldsymbol{K\eta^{-3}}$ ∞ $-\frac{1}{2}K^2\eta^{-8/3}$

TABLE 1. Fixed points for $\delta \neq 0, 1$: position and properties of the fixed points of the autonomous system (3.11) for $\delta \neq 0, 1$. UF denotes an unstable focus, SF a stable focus, UN an unstable node, SN a stable node, S a saddle and S–N a saddle–node. The entries for $v(\eta)$ and $z(\eta)$ are the asymptotic expansions about the fixed point, where K and K' are constants of integration. The first two lines for each fixed point are relevant to the eigenvector curves. If a third line is given, it corresponds to generic curves. Entries in bold are exact analytic values. From these expansions, those for u, $\hbar$ and $2\pi ru\hbar$ can be obtained via (3.12). The values of the constants in the table are $\delta_\pm = (2 \pm \sqrt{2})/4$, $\delta_\pm^* = (7 \pm \sqrt{7})/14$, $\alpha_\pm = (3 \pm \sqrt{64\delta^2 - 64\delta + 17})/(8\delta^2 - 8\delta + 1)$ and $v_1 = (1 + \sqrt{8\delta^2 - 8\delta + 1})/2\delta$, $v_2 = (1 - \sqrt{8\delta^2 - 8\delta + 1})/2\delta$ with $z_{1,2} = [(1-2\delta)v_{1,2} + 3\delta - 2]/\delta$.

Fixed point	δ	η	u	$\hbar$	$2\pi r u \hbar$
O	$(-\infty, 0)$	0	0	0	0
	$(0, 1)$	∞	0	0	0
	$(1, \infty)$	∞	∞	0	0
	$(-\infty, 0)$	0	0	0	0
	$(0, 1)$	∞	0	0	0
	$(1, 2)$	∞	0	∞	∞
	$(2, \infty)$	∞	∞	∞	∞
	$(-\infty, 0)$	0	0	0	0
	$(0, \frac{3}{4})$	∞	0	0	0
	$(\frac{3}{4}, 1)$	∞	0	0	∞
	$(1, \infty)$	∞	∞	∞	∞
A	$(-\infty, \infty)$	f	f	0	0
B	$(-\infty, 1)$	∞	∞	0	0
	$(1, \infty)$	0	0	0	0
	$(-\infty, 0)$	∞	∞	∞	∞
	$(0, \frac{1}{2})$	∞	∞	0	∞
	$(\frac{1}{2}, 1)$	∞	∞	0	0
	$(1, \infty)$	0	0	0	0
C_1	$(-\infty, \delta_-), (\delta_+, \infty)$	f	f	f	f
C_2	$(-\infty, \delta_-), (\delta_+, \infty)$	f	f	f	f
D	$(-\infty, \infty)$	∞	∞	∞	∞
	$(-\infty, \delta_-)$	0	0	0	0
	(δ_-, δ_+)	∞	∞	∞	∞
	(δ_+, ∞)	0	0	0	0
E	$(-\infty, \infty)$	∞	∞	∞	∞
	$(-\infty, \infty)$	0	0	f	0
F	$(-\infty, \infty)$	∞	∞	0	∞
	$(-\infty, \infty)$	0	f	0	0
G	$(-\infty, \infty)$	0	∞	∞	∞
	$(-\infty, \infty)$	0	∞	∞	∞
	$(-\infty, \infty)$	0	∞	∞	f

TABLE 2. Fixed points for $\delta \neq 0, 1$: values of η, u, $\hbar$, and $2\pi r u \hbar$ at the fixed points of the autonomous system (3.11) for $\delta \neq 0, 1$. For each fixed point, each subsection of the table relates to the corresponding line in table 1. Where there is only a single subsection, the solutions in all the lines of table 1 have the same value at the fixed point. Here f corresponds to a finite, non-zero value and $\delta_\pm = (2 \pm \sqrt{2})/4$.

tables it can be seen that there is a single fixed point which corresponds to (3.7), and it is the origin O when $0 < \delta \leqslant 1$.

3.6. *The critical parabola*

Before investigating how solutions change with changing δ, we discuss how to ensure that a solution given by an integral curve in the phase plane is physically meaningful. For this, we must consider the curve $\mathscr{P}_c$,

$$z = (v - 1)^2, \tag{3.13}$$

referred to as the critical parabola (see Gratton & Vigo 1994). This curve is important because the change of variables from η to λ removes the singularities which exist for η on $\mathscr{P}_c$, or alternatively, η changes direction with respect to λ when (and only when) an integral curve crosses $\mathscr{P}_c$. Because λ is monotonic on any integral curve, this implies that v and z, and hence u and $\hbar$, become multivalued functions of η. This is clearly not a stable physical state and therefore we do not consider integral curves which cross the critical parabola.

It is still possible for points on either side of the critical parabola to be connected in a physically meaningful way. For this, η must be monotonic and thus λ cannot be monotonic: the solution must approach $\mathscr{P}_c$ with λ monotonically increasing (or

Fixed point	v	z	Type in λ	$v(\eta)$	$z(\eta)$	η	u	$\hbar$	$2\pi ru\hbar$
O	0	0	UN	$\mathbf{0}$	$\boldsymbol{K\eta^{-2}}$	∞	0	f	0
				$\boldsymbol{K\eta^{-1}}$	$\mathbf{0}$	∞	f	0	0
				$K\eta^{-1}$	$K'\eta^{-2}$	∞	f	f	∞
A	1	0	D	$1+\frac{2}{3}(1+K\eta)$	$\frac{1}{9}(1+K\eta)^2$	f	f	0	0
				$\boldsymbol{K\eta^{-1}}$	$\mathbf{0}$	f	f	0	0
C	0	1	SN	$\mathbf{0}$	$\boldsymbol{K\eta^{-2}}$	f	0	f	0
				$\frac{1}{3}(K\eta-1)$	$1-\frac{5}{3}(K\eta-1)$	f	0	f	0
D	$\frac{1}{2}$	$\frac{1}{8}$	S	$\frac{1}{2}+K\eta^{3-\sqrt{17}}$	$\frac{1}{8}-\frac{1+\sqrt{17}}{8}K\eta^{3-\sqrt{17}}$	∞	∞	∞	∞
				$\frac{1}{2}+K\eta^{3+\sqrt{17}}$	$\frac{1}{8}-\frac{1-\sqrt{17}}{8}K\eta^{3+\sqrt{17}}$	0	0	0	0
E	0	∞	S	$\mathbf{0}$	$\boldsymbol{K\eta^{-2}}$	0	0	f	0
				$\boldsymbol{K\eta^{-2}}$	∞	∞	0	∞	∞
F	∞	0	S	∞	$\boldsymbol{K\eta^{-3}}$	∞	∞	0	∞
				$\boldsymbol{K\eta^{-1}}$	$\mathbf{0}$	0	f	0	0
G	∞	∞	S–N	∞	$\boldsymbol{K\eta^{-3}}$	0	∞	∞	∞
				$\boldsymbol{K\eta^{-2}}$	∞	0	∞	∞	∞
				$K\eta^{-\frac{4}{3}}$	$-\frac{1}{2}K^2\eta^{-\frac{8}{3}}$	0	∞	∞	f

TABLE 3. Fixed points for $\delta = 1$: position and properties of the fixed points of the autonomous system (3.11) for $\delta = 1$. UN denotes an unstable node, SN a stable node, S a saddle, S–N a saddle–node and D some other degenerate fixed point. The entries for $v(\eta)$ and $z(\eta)$ are the asymptotic expansions about the fixed point, where K and K' are constants of integration. The first two lines for each fixed point are relevant to the eigenvector curves. If a third line is given, it corresponds to generic curves. Entries in bold are exact analytic values. From these expansions, those for u, $\hbar$ and $2\pi ru\hbar$ can be obtained via (3.12) and the entries for these variables are their values at the fixed point, where f has a finite, non-zero value.

decreasing) and leave with λ monotonically decreasing (or increasing). This can occur at a fixed point of (3.11) such as point C_1 or C_2 of figure 2(*b*).

Another way to overcome the restriction on crossing the critical parabola is to allow jumps, because these connect integral curves on either side of the critical parabola. Consider $Fr_s'^2 = (v'-1)^2/z'$ and $Fr_s^2 = (v-1)^2/z$, then from (3.9) we see that

$$Fr_s'^2 = \frac{8}{\phi^3}Fr_s^2 = \frac{\phi+2}{\phi^2}, \tag{3.14}$$

where $\phi = \phi(Fr_s)$. If the point (v', z') ahead of the shock lies above the parabola, then $Fr_s'^2 < 1$ and from (3.9) and (3.14) we see that $Fr_s^2 > 1$. Similarly, it can be shown that $Fr_s'^2 > 1$ implies $Fr_s^2 < 1$. Hence the jump condition connects points which are supercritical (have $Fr_s > 1$ and lie below $\mathscr{P}_c$) with points which are subcritical (have $Fr_s < 1$ and lie above $\mathscr{P}_c$) and vice versa. Points on $\mathscr{P}_c$ are mapped into themselves.

3.7. *Phase-plane solution*

In § 3.5, we determined the points in the (v, z) phase plane which correspond to the boundary conditions (2.2) and (2.7). These are the origin O and $(1, 1/Fr^2)$ respectively. We now need to find the value of $\delta \in (0, 1]$ for which an integral curve, or appropriate set of integral curves, connects these points.

The fixed point $(1, 1/Fr^2)$ and O lie on either side of the critical parabola. Therefore, as discussed in the last subsection, we have the problem of how to connect them.

In analogous problems in gas dynamics and cavitation, it has been assumed that u and h must be regular everywhere (see Hunter 1960, 1963). The argument is that any discontinuities must be created in the system very precisely for them to propagate in a self-similar way; and this is regarded as unrealistic. In order to confirm this we studied the results of a numerical scheme for the initial value problem (which we describe in § 4). For all the initial height profiles which we tried, the profiles of u and h appear smooth close to collapse; any shocks which were present propagated through the profile and were no longer important. This does not rule out the possibility of creating similarity solutions with discontinuities, and Gratton (1991) has suggested pursuing such solutions. However, it does suggest that the most relevant similarity solutions are those that are smooth and we restrict ourselves to these. This restriction disallows the possibility of connecting the integral curves through $(1, 1/Fr^2)$ and O with jumps according to (3.9).

This leaves us with having to connect $(1, 1/Fr^2)$ and O via a fixed point on the critical parabola. From tables 1 and 3 we see that C_1 and C_2 are the two possible fixed points, both of which are nodes for $\delta \in (0, 1]$, if they exist. We need to ensure that the curve we choose through C_1 or C_2 has u and h regular, which is easily seen to be true when $\mathrm{d}v/\mathrm{d}z$ is regular.

We define the major-axis solution to be the eigenvector curve along which generic curves enter the fixed point tangentially and define the minor-axis solution to be the other eigenvector curve. Then, following the same analysis as given in Hunter (1960), we can show for both C_1 and C_2 that the minor-axis solution is always regular for $\delta \in (0, 1]$. For the major-axis solution, the situation is slightly more complicated. For most values of δ, the solution is regular but none of the remaining curves entering C_1 and C_2 are regular. However, for at most countably many values of δ, either none of the curves tangent to this eigenvector are regular or all of them are. We do not consider the case where all are regular because there are then several conditions on δ and we do not expect it to be possible to satisfy them all. This is a slightly unsatisfactory reason. However, it turns out to be acceptable in that the value of δ which we choose from the phase-plane analysis, under this restriction, matches closely with the value obtained from initial value problems (which we give in § 4). We therefore choose δ such that the curve connecting O with $(1, 1/Fr^2)$ passes through the relevant fixed point, C_1 or C_2, along either the minor- or the major-axis solution.

Unless the curve enters the fixed point along either the minor- or the major-axis solution, it changes direction very abruptly close to the critical parabola, which is seen in curves P_1 and P_2 in figure 2 (*b*). This behaviour allowed us to use a numerical shooting technique to find the correct value of δ. We integrated (3.10) and (3.11), using the fourth-order Runge–Kutta scheme of *ODE Architect*, from $(1, 1/Fr^2)$ to the appropriate fixed point. We then varied the value of δ until the curve entered the fixed point along the minor-axis solution. The curves cannot enter the fixed points along the major-axis solution for $Fr \in (0, \infty)$, as indicated in figure 2 (*b*). They could enter along the major-axis curve if they originate at A, a situation which we do not discuss since we are mainly interested in finite Froude numbers, or E, which is not relevant.

For the experimentally determined frontal Froude number, for the Boussinesq case, of 1.19, $\delta = 0.859094$ and the velocity and height profiles are as shown in figure 3. At

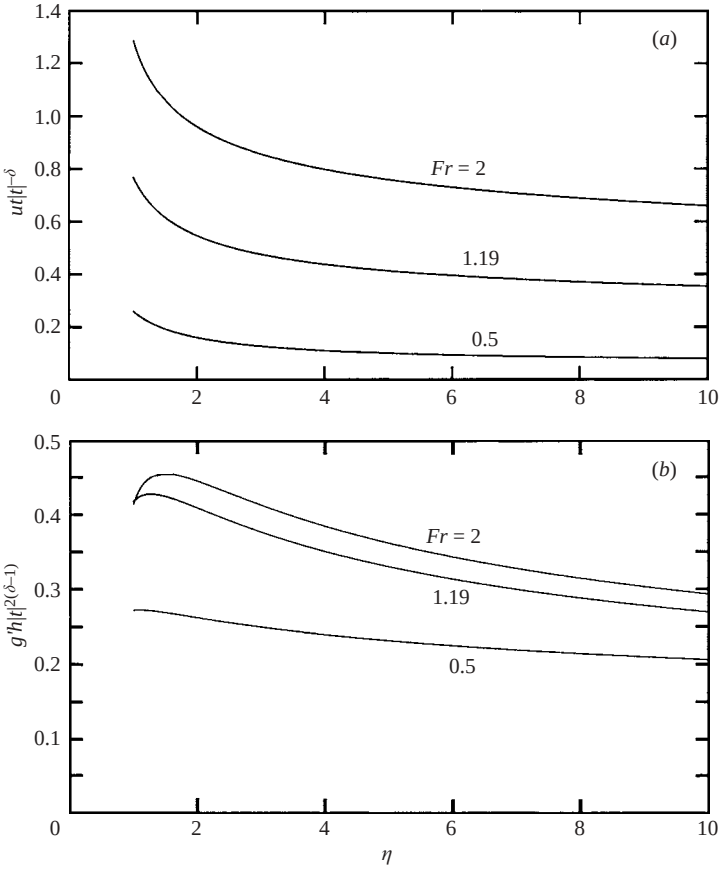

FIGURE 3. (*a*) Velocity and (*b*) height profiles for different values of the frontal Froude number. The value of b used is that found by following the initial value problem ($R_o = 10$, $\hbar_i = 1.0$, see § 4) until it reaches the self-similar regime.

the front, the values of the height, and speed are seen to be significantly higher than their values at infinity. This may be expected since the narrowing of the geometry forces fluid to pile up, increasing the height, and the greater head of fluid produces greater fluid speeds at the front. This behaviour was seen both experimentally and numerically by Hallworth *et al.* (2003). What was not described in their paper was the curling over at the front: very close to the front, the height decreases again. This feature can also be explained. From the shallow-water equations (2.1) we have that

$$\frac{\mathrm{D}u}{\mathrm{D}t} = -\frac{\partial \hbar}{\partial r}. \tag{3.15}$$

Hence for the front to accelerate (increased negative velocity) due to the narrowing of the geometry, we require $\partial \hbar/\partial r > 0$ at the front.

For other Froude numbers, the value of δ is different and figure 4 shows the behaviour of δ with Froude number. For $Fr < Fr_c \simeq 1.75$, the appropriate curve from $(1, 1/Fr^2)$ to O passes through C_2 whereas for $Fr > Fr_c$, the curve passes through C_1. At $Fr = Fr_c$, C_1, C_2 and D merge, in a pitchfork bifurcation, at $(1/2\delta_c, 1/8\delta_c^2)$ where $\delta_c = (2 + \sqrt{2})/4$. For each $Fr \in (0, \infty)$, the value of δ, and hence also the solution,

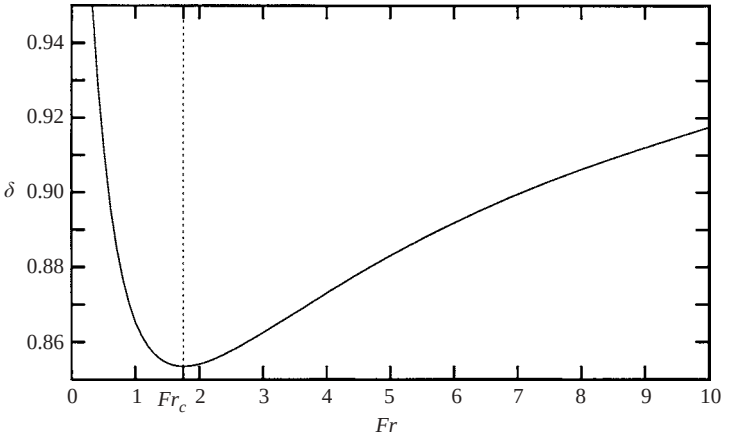

FIGURE 4. Similarity exponent, δ, versus frontal Froude number. The critical Froude number is $Fr_c \simeq 1.75$. The minor-axis solution passes through C_2 for smaller Froude numbers and through C_1 for larger Froude numbers (see figure 2).

is unique. However, for $Fr = \infty$, for any $\delta \in (0, 1]$, $z = 0$ is a solution and for $Fr = 0$ there are no regular solutions.

It is also of interest to determine how the velocity and height profiles change with Froude number. These changes in behaviour are shown in figure 3. For all Froude numbers we have

$$\left.\frac{\partial h}{\partial r}\right|_{r=r_f} = \delta^2 b|t|^{\delta-2} \left.\frac{\mathrm{d}}{\mathrm{d}\eta}(\eta^2 z)\right|_{\eta=1} \tag{3.16a}$$

$$= \delta(1-\delta)b|t|^{\delta-2} > 0, \tag{3.16b}$$

which indicates a curling over of the front. We cannot say how large this gradient is purely from the similarity analysis because b can only be found from numerical evaluation or experiment. From initial value investigations, the curling over is seen to reduce as $Fr \to 0$ and increase as $Fr \to \infty$ for the same initial configuration. This may be explained from the fact that small Froude numbers correspond to large ambient resistance to the advance of the gravity current and hence the acceleration of the front is small. For large Froude numbers the ambient provides little resistance to the current, because its density is much lower, and hence the acceleration of the front is greater.

As the Froude number increases, the maximum in both the speed and height profiles increases. This may also be expected since lower ambient resistance to flow allows greater velocities and heights to develop.

3.8. *Special case of* $\delta = 0$

We now investigate the phase plane for $\delta = 0$. Solutions for $\delta = 0$ may be called quasi-steady (Jensen 1994) since t only occurs in the scalings of u and h and not in η. In this case, the forms for u and h in (3.3) are not appropriate. Instead we set

$$u = \frac{r}{t}V(\eta), \quad h = \frac{r^2}{t^2}Z(\eta), \tag{3.17}$$

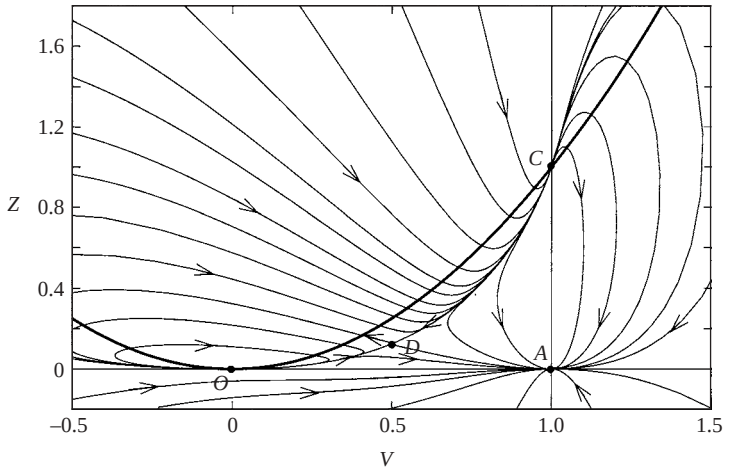

FIGURE 5. The (V, Z) phase plane for $\delta = 0$. The arrows indicate the direction of increasing η. The bold curve is the critical parabola $Z = V^2$.

where $\eta = r/b$, and the phase-plane equations become

$$\frac{\mathrm{d}\log\eta}{\mathrm{d}\Lambda} = Z - V^2, \tag{3.18a}$$

$$\frac{\mathrm{d}V}{\mathrm{d}\Lambda} = (1 - V)(2Z - V^2), \tag{3.18b}$$

$$\frac{\mathrm{d}Z}{\mathrm{d}\Lambda} = Z(3V^2 - V - 2Z). \tag{3.18c}$$

The boundary condition at the outer cylinder (3.7) is $u \to 0$, or equivalently $V \to 0$, as $\eta \to f$ where f has some finite, non-zero value. The boundary condition at the front (3.8) remains unchanged. Hence we need to find an integral curve that connects the line $V = 0$ with the line $V = 1$.

Figure 5 shows a plot of the (V, Z) phase plane. Note that in this case, the critical parabola becomes $Z = V^2$ from (3.18*a*). As can be seen, it is not possible to connect the lines $V = 0$ and $V = 1$ without crossing the critical parabola, unless we connect O with the fixed point C via the saddle D, or O with A. For the former case, from table 4 we see that along this curve entering D, η becomes infinite at D whereas at O and C, η is finite. Therefore on this curve, $V(\eta)$ and $Z(\eta)$ are clearly multivalued. For the latter case, η increases from O to A which is physically unrealistic. Hence it is not possible to satisfy both boundary conditions for $\delta = 0$ when requiring a physically realistic solution.

4. Comparison with the initial value problem

It is important to ascertain how the intermediate asymptotics given by the similarity solution of the previous section compare to the solution of an initial value problem.

To investigate this, we used a numerical code which has previously been used by Hallworth *et al.* (2003) to study the initial value problem for an inwardly propagating, inviscid, axisymmetric gravity current. Here we set $t = 0$ to be the time at which the flow is initiated, and the shallow-water equations (2.1) are integrated from initial

Fixed point	V	Z	Type in Λ	$V(\eta)$	$Z(\eta)$	η	u	$\hbar$	$2\pi r u \hbar$
O	0	0	D	$\mathbf{1 + K\eta^{-1}}$	$\mathbf{0}$	f	0	0	0
				$\frac{2}{3}(K\eta - 1)$	$\frac{1}{9}(K\eta - 1)^2$	f	0	0	0
A	1	0	UN	$\mathbf{1 + K\eta^{-1}}$	$\mathbf{0}$	∞	∞	0	0
				$\mathbf{1}$	$\mathbf{K\eta^{-2}}$	∞	∞	f	∞
				$1 + K\eta^{-1}$	$K'\eta^{-2}$	∞	∞	f	∞
C	1	1	SN	$\mathbf{1}$	$\mathbf{K\eta^{-2}}$	f	f	f	f
				$1 + \frac{1}{3}(1 + K\eta)$	$1 + \frac{5}{3}(1 + K\eta)$	f	f	f	f
D	$\frac{1}{2}$	$\frac{1}{8}$	S	$\frac{1}{2} - \frac{1-\sqrt{17}}{2} K\eta^{3-\sqrt{17}}$	$\frac{1}{8} + K\eta^{3-\sqrt{17}}$	∞	∞	∞	∞
				$\frac{1}{2} - \frac{1+\sqrt{17}}{2} K\eta^{3+\sqrt{17}}$	$\frac{1}{8} + K\eta^{3+\sqrt{17}}$	0	0	0	0
E	1	∞	S	$\mathbf{1}$	$\mathbf{K\eta^{-2}}$	0	0	f	0
				$\mathbf{1 + K\eta^{-2}}$	$\mathbf{\infty}$	∞	∞	∞	∞
F	∞	0	S	$\mathbf{\infty}$	$\mathbf{K\eta^{-3}}$	∞	∞	0	∞
				$\mathbf{1 + K\eta^{-1}}$	$\mathbf{0}$	0	f	0	0
G	∞	∞	S–N	$\mathbf{\infty}$	$\mathbf{K\eta^{-3}}$	0	∞	∞	∞
				$\mathbf{1 + K\eta^{-2}}$	$\mathbf{\infty}$	0	∞	∞	∞
				$K\eta^{-\frac{4}{3}}$	$-\frac{1}{2}K^2\eta^{-\frac{8}{3}}$	0	∞	∞	f

TABLE 4. Fixed points for $\delta = 0$: position and properties of the fixed points of the autonomous system (3.18) for $\delta = 0$. UN denotes an unstable node, SN a stable node, S a saddle, S–N a saddle–node and D some other degenerate fixed point. The entries for $V(\eta)$ and $Z(\eta)$ are the asymptotic expansions about the fixed point, where K and K' are constants of integration. The first two lines for each fixed point are relevant to the eigenvector curves. If a third line is given, it corresponds to generic curves. Entries in bold are exact analytic values. From these expansions, those for u, $\hbar$ and $2\pi r u \hbar$ can be obtained and the entries for these variables are their values at the fixed point, where f has a finite, non-zero value.

velocity and height distributions given by

$$u = 0, \quad 0 \leqslant r \leqslant R_o, \tag{4.1a}$$

$$\hbar = \begin{cases} 0, & 0 \leqslant r < R_o - 1 \\ \hbar_i(r), & R_o - 1 \leqslant r \leqslant R_o, \end{cases} \tag{4.1b}$$

where variables have been non-dimensionalized using typical length- and timescales. In general the initial height $\hbar_i = 1$ but we also chose different height profiles to investigate how the similarity solution depends on the precise initial conditions. A boundary condition of zero velocity is applied at $r = R_o$ and a constant Froude number condition is applied at the front (cf. (2.2) and (2.7)). Details of the numerical method and non-dimensionalization are given in Hallworth *et al.* (2003).

To study the transition to self-similarity, we consider the front position against time. Figure 6 shows a log–log plot of the front position against $1 - t/t_c$ for $Fr = 1.19$, $\hbar_i = 1$ and $R_o = 10$. Here t_c is the time of collapse and is taken as the time at which the front position first becomes non-positive. For times very close to collapse, the numerical scheme begins to fail, as can be seen by the increasing spread of results for different time steps and grid spacings as $t \to t_c$. For times close to initiation (t close to 0) the self-similar regime will not yet have been reached. Hence we take, somewhat arbitrarily, only front positions which correspond to $1 - t/t_c \in (0.01, 0.1)$

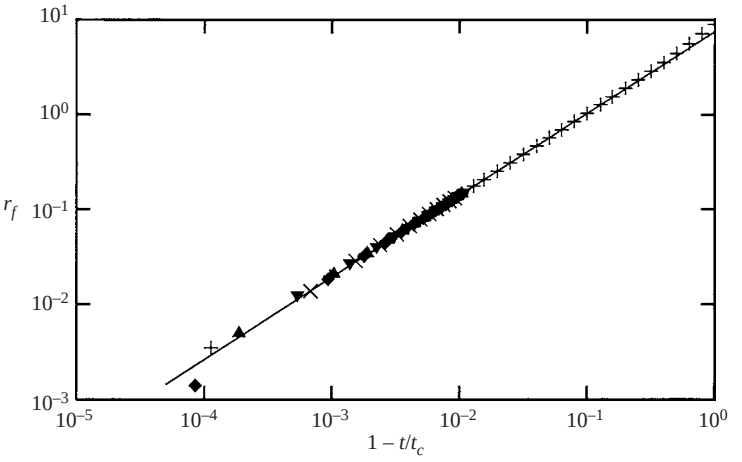

FIGURE 6. Front position r_f versus $1 - t/t_c$ for the numerical solution of the initial value problem with initial height profile $h_i = 1$, outer cylinder radius $R_o = 10$ and $Fr = 1.19$. The line is the line of best fit, given by (4.2). The five different symbols are solutions for different accuracies to display the increasing spread as $t \to t_c$ (see below). For $1 - t/t_c > 0.01$ only the most accurate run has been plotted, at selected points, as the solution for different accuracies overlie one another. As $t \to 0$ it can be seen that the solution diverges from the line of best fit. $\times$, $\Delta t = 10^{-3}$, $\Delta y = 1/200$; $\blacktriangledown$, $\Delta t = 10^{-3}$, $\Delta y = 1/400$; $\blacktriangle$, $\Delta t = 10^{-4}$, $\Delta y = 1/400$; $\blacklozenge$, $\Delta t = 10^{-4}$, $\Delta y = 1/800$; $+$, $\Delta t = 10^{-5}$, $\Delta y = 1/800$;

as representing self-similarity, although the precise choice does not greatly affect the result. A least-squares fit through these points, for the run of highest accuracy ($\Delta t = 10^{-5}$, $\Delta y = 1/800$) then gives

$$\delta = 0.864, \tag{4.2a}$$

$$b = r_f|_{t=0} / t_c^{\delta} = 0.898, \tag{4.2b}$$

where b is non-dimensional, since the equations have been non-dimensionalized, and $r_f|_{t=0}$ is the value obtained from the least-squares fit. This value of δ is within 0.5% of the value calculated theoretically in the previous section. We found a similar degree of accuracy for other values of the Froude number.

Figures 7(a) and 7(b) show the velocity and height profiles, scaled with $r_f/(t_c - t)$ and $r_f^2/(t_c - t)^2$ respectively, before collapse for $Fr = 1.19$ compared to the self-similar regime. The profiles suggest that the initial value problem asymptotically approaches the similarity solution we have found. However, it should be noted that the approach is non-uniform, with agreement better close to the front.

Overall, the fit appears to be reasonably good. Certainly the value obtained for δ is very close to the theoretically obtained value. However, the numerics fail as we get closer to the instant of collapse so it is not possible to check for a closer fit as $t \to t_c$. At such times it would have been better either to use a higher-order numerical scheme or one with an adaptive mesh, or to use a renormalization technique such as is given in Chen & Goldenfeld (1995). The renormalization technique can be much faster and so allows greater accuracy; however, it does not allow an investigation of the stages leading to self-similarity as direct numerical integration does. We have not pursued a more accurate method because the fit we have obtained is sufficiently reasonable.

We have also performed computations with different initial height profiles but the same cylinder radii and fluid volume. All reach the self-similar form to within the

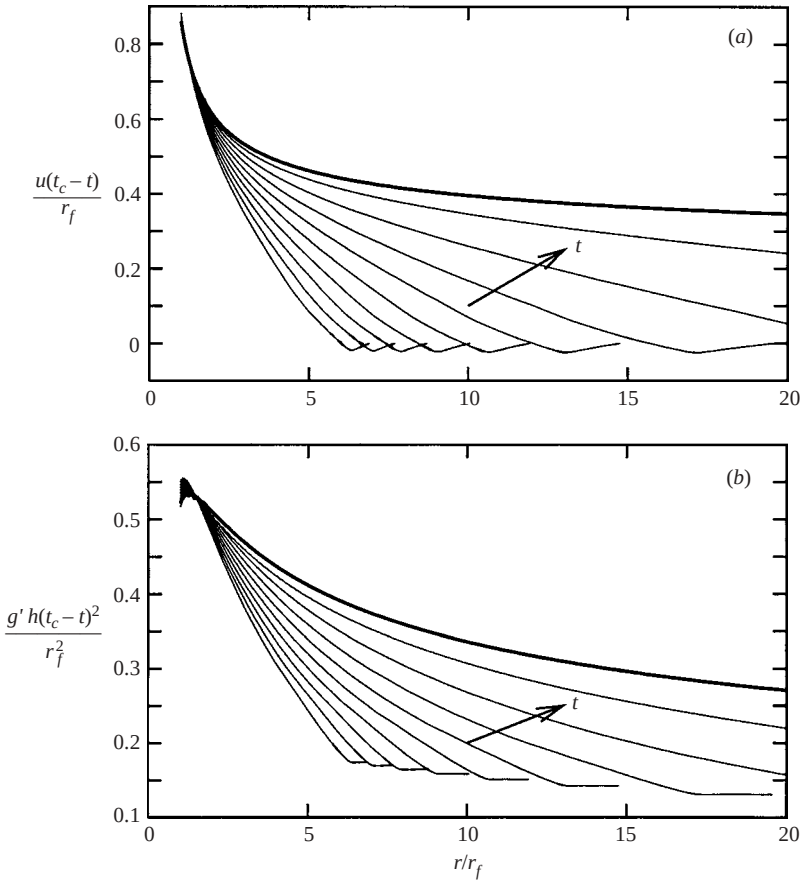

FIGURE 7. Non-dimensional profiles of (*a*) velocity and (*b*) height versus η comparing the numerical results of the initial value problem close to collapse with the similarity solution. The numerical solution is plotted for $t = 10$ to $t = 11.6$ in intervals of 0.2 and collapse occurs at $t = 11.72$. The arrow indicates solutions at increasing time. The thicker curve represents the similarity solution. Note that it is only very close to the time of collapse that the similarity solution is a good approximation.

accuracy we have just described. This suggests some stability of the self-similar form to varying initial conditions. The values of b are also identical to within numerical error and suggest that this is an initial condition which is forgotten by the system (contrary to what was concluded for viscous currents by Diez, Gratton & Gratton 1992*b*).

A dependence of the value of b on the volume and radius of the outer cylinder was suggested in § 3 and is illustrated in table 5. As the radius of the outer cylinder is increased for a fixed volume, the value of t_c increases and hence, from (4.2 *b*), b decreases. Similarly, as the volume is increased for a fixed radius, the value of t_c decreases as the greater head of fluid causes greater fluid velocities, and b is increased.

5. Self-similar behaviour at and after collapse

In this section we briefly discuss the behaviour at and after collapse. In contrast to the similarity solution before collapse, the similarity solution afterwards can only

R_o	$\hbar_i$	$g'V/2\pi$	δ	b	t_c
10	0.5	19/4	0.86349	0.679	16.2
10	1.0	19/2	0.86357	0.898	11.7
10	2.0	19	0.86359	1.15	8.35
8	19/15	19/2	0.86355	1.07	7.59
12	19/23	19/2	0.86354	0.764	17.3
14	19/27	19/2	0.86354	0.710	22.2

TABLE 5. Values of δ, b and t_c for different initial heights and outer cylinder radii. The value of δ is very consistent for the different runs.

be expected to be valid at times close to its initiation. This is because it is only possible to create solutions with a shock and, as discussed in § 3.7, these are likely to be unstable features of the flow.

We return to setting $t=0$ to be the time of collapse. At $t=0$ the front reaches the origin and for times shortly afterwards, the information about collapse will not have reached the far field and hence only the flow at $r=0$ should be immediately affected. This implies that for the solution at $t=0$ and for the similarity solution for $t>0$ the exponent δ in the variable η should be the same as before collapse. In addition, $u(\eta)$ and $\hbar(\eta)$ before and after collapse should match in the limit $\eta\to\infty$.

First we consider the behaviour at the instant of collapse. From (3.3) we can write

$$u=\delta b^{1/\delta}r^{1-1/\delta}\eta^{1/\delta}v(\eta),\quad \hbar=\delta^2 b^{2/\delta}r^{2-2/\delta}\eta^{2/\delta}z(\eta). \tag{5.1}$$

From table 1, $\eta^{1/\delta}v(\eta)\to K$ and $\eta^{2/\delta}z(\eta)\to K'$ as $\eta\to\infty$ before collapse. Hence at collapse

$$u=\delta b^{1/\delta}Kr^{1-1/\delta},\quad \hbar=\delta^2 b^{2/\delta}K'r^{2-2/\delta}. \tag{5.2}$$

The profiles of $u(r)$ and $\hbar(r)$ at $t=0$ for $Fr=1.19$ are shown in figures 8(a) and 8(b) respectively. Note that both the height and the speed tend to infinity as r tends to 0.

We now look for a similarity solution after collapse. We still consider the (v,z) phase plane for the same value of δ. However, the points between which we wish to find an integral curve may have changed to reflect the new configuration and hence new boundary conditions. In fact, the far-field boundary condition (3.7), at $\eta=\infty$, cannot have changed and hence O is still the appropriate fixed point in the phase plane. However, the boundary condition (3.8) is no longer relevant. Instead we require that

$$u\to 0,\quad \hbar\to f \tag{5.3}$$

as $\eta\to 0$, where f has some finite non-zero value. As discussed in § 3.5, η can only tend to zero at the fixed points of the system (3.11). The fixed point at which (5.3) holds is E at $(1/\delta-1,\infty)$ (see table 2). Hence we must find an integral curve connecting O and E for the same value of δ as before collapse.

The additional restriction that u and $\hbar$ remain unchanged in the limit $\eta\to 0$ gives the integral curve leaving O. Close to O (the point corresponding to $\eta=\infty$) the integral curves in the phase plane are given by $z\sim(\hbar/u^2)v^2$. Therefore the integral curve emanating from O after collapse must lie on the same parabola as before collapse, although for $t>0$ and $u<0$ we require $v<0$ compared to $v>0$ for $t<0$. We can obtain an initial condition for the system of differential equations (3.10) and (3.11) by setting

$$\eta=\eta_i,\quad v_a(\eta_i)=-v_b(\eta_i),\quad z_a(\eta_i)=z_b(\eta_i), \tag{5.4}$$

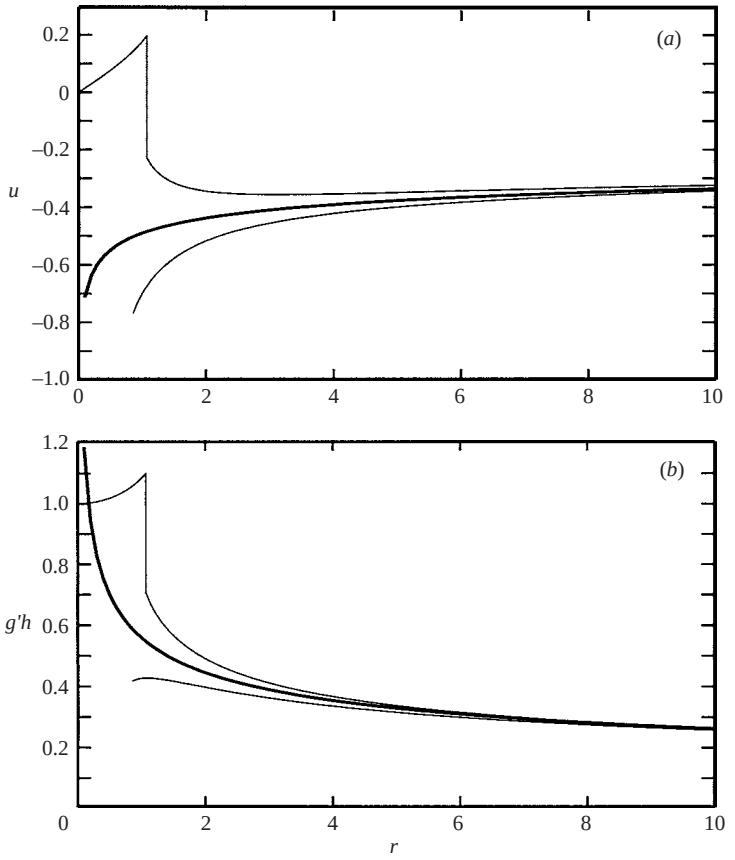

FIGURE 8. (*a*) Velocity and (*b*) height profiles versus r for $Fr = 1.19$. The profile before collapse (the bottom curve in both plots) is given at $t = -1$ and that after collapse (the top curve in both plots) at $t = 1$. The profile at collapse is given by the thicker curve. As $r \to 0$, the velocity at collapse tends to $-\infty$ and the height to $+\infty$. The value of b used is that found by following the initial value problem ($R_o = 10$, $\hbar_i = 1.0$, see § 4) until it reaches the self-similar regime.

where η_i is some large value and subscript a denotes the solution after collapse and b denotes the solution before collapse. A more accurate scheme could be derived using Taylor series.

This integral curve leaving O does not enter E and hence the only way to connect the two points is with a jump. However, we do not yet know where the jump should be. So now we consider the integral curve leaving E. This fixed point is a saddle with only one eigenvector curve entering the finite plane. Using a five-term Taylor series expansion about this point, we can start a numerical integration along this integral curve. As yet, there is not a condition on η; however, the system (3.4) is autonomous and hence it can be set arbitrarily for the moment. We can then map this curve onto a curve of the corresponding points after a jump, using (3.9). The position of the intersection between this mapped curve and the integral curve from O gives us the (v, z) coordinates of the jump and also the value of η there. From this the full solution can be obtained.

The profiles of $u(r)$ and $\hbar(r)$ at $t = 1$ are shown in figures 8(*a*) and 8(*b*) respectively. For large r, both the velocity and height are seen to converge to their profiles before

(and at) collapse. An appreciable shock has appeared in the solution after collapse with the height attaining its maximum at the shock.

6. Conclusions

Using the phase-plane method, we have investigated the existence of similarity solutions with converging fronts of the axisymmetric shallow-water equations, modelling inviscid, inwardly propagating gravity currents. We imposed the condition of regularity of height and velocity (consistent with analysis done of imploding shocks in gas dynamics). Under this restriction:

(*a*) there is a unique similarity solution for all frontal Froude numbers, $Fr \in (0, \infty)$;

(*b*) there are uncountably many similarity solutions for $Fr = \infty$; and

(*c*) there are no solutions for $Fr = 0$, corresponding to the propagation of a gravity current of zero density into an ambient fluid of finite density.

For all finite, non-zero values of the frontal Froude number, the speed and height increase monotonically towards the front, although the height decreases again slightly just at the front. With increasing Froude number, the maxima in both the speed and height increase, reflecting the decrease in ambient resistance as the density of the current increases relative to that of the ambient. The gradient of the height at the front also increases as the Froude number increases for the same reason, since it is equal to the acceleration of the front.

We have compared the similarity solution to the numerical solution of the initial value problem in Hallworth *et al.* (2003). The fit is reasonably good, with the similarity exponent found less than 0.5% away from the true value. The height and velocity profiles appear to converge to the similarity solution at times near collapse, with an especially close fit in the region of the front. However, the numerical scheme used begins to fail close to collapse and a different scheme may achieve a closer fit.

We have also considered the solution at collapse, for which the height and speed are infinite at the origin. After collapse, we have found the relevant similarity solution, which has an appreciable shock.

We now briefly address the question of the physical relevance of the solutions we have found. As a first approximation, our similarity solutions do capture the most significant features. However, the shallow-water equations are likely to become inaccurate as the front approaches the origin because vertical motion becomes significant. Also, some aspects of real gravity currents have been neglected in the simplified model which we have used. The complex three-dimensional structure of the head, turbulent mixing, entrainment, friction and so on are all present to some extent. The constancy of the Froude number is essential in the analysis employed to obtain the similarity solution, but it is not always a good approximation.

As a final remark, the axisymmetric currents may not be stable. In a related problem, where a vertical jet impinges on a flat surface and a moderate Reynolds number outflowing current results, an interesting instability has been observed. An axisymmetric hydraulic jump is created in the flow; however, it may undergo symmetry breaking and form a stationary polygonal shape (Ellegaard *et al.* 1999). In a more closely related problem, imploding axisymmetric shock waves in gas dynamics have also been shown to be unstable and become polygonal (see Whitham 1956; Schwendeman & Whitham 1987; Betelú & Aronson 2001) and a similar analysis would be interesting for the shallow-water equations. Although the governing equations of gas dynamics for adiabatic exponent 2 and the shallow-water equations are identical, the jump conditions are different and also the frontal Froude number condition is

very different from the formulation used in gas dynamics and could be a stabilizing effect. We have not performed such an analysis but it might be interesting to do so in the future.

The authors are grateful to Marius Ungarish for supplying the numerical code used in the investigation of the initial value problem and to G. I. Barenblatt, J. Gratton, A. Acrivos, N. Goldenfeld, S. I. Betelú, H. A. Stone, M. Ungarish and M. G. Worster for stimulating comments on an earlier version of this work. This research was partially supported by a PhD studentship to A. C. S. from NERC, award number NER/S/A/2002/10337.

REFERENCES

Aronson, D. G. & Graveleau, J. 1993 A selfsimilar solution to the focusing problem for the porous medium equation. *Eur. J. Appl. Maths* **4**, 65–81.

Barenblatt, G. I. 1996 *Scaling, Self-similarity and Intermediate Asymptotics*. Cambridge University Press.

Benjamin, T. B. 1968 Gravity currents and related phenomena. *J. Fluid Mech.* **31**, 209–248.

Betelú, S. I. & Aronson, D. G. 2001 Focusing of noncircular self-similar shock waves. *Phys. Rev. Lett.* **87**, art. no. 074501.

Bilbao, L. E. & Gratton, J. 1996 Spherical and cylindrical convergent shocks. *Nuovo Cimento* **18D**, 1041–1060.

Brushlinskii, K. V. & Kazhdan, J. M. 1963 On auto-models in the solution of certain problems of gas dynamics. *Russ. Math. Surv.* **18** (2), 1–22.

Chen, L.-Y. & Goldenfeld, N. 1995 Numerical renormalization-group calculations for similarity solutions and traveling waves. *Phys. Rev.* E **51**, 5577–5581.

Diez, J. A., Gratton, J. & Minotti, F. 1992*a* Self-similar solutions of the second kind of nonlinear diffusion-type equations. *Q. Appl. Maths* **L** (3), 401–414.

Diez, J. A., Gratton, R. & Gratton, J. 1992*b* Self-similar solution of the second-kind for a convergent viscous gravity current. *Phys. Fluids* A **4**, 1148–1155.

Ellegaard, C., Hansen, A. E., Haaning, A., Hansen, K., Marcussen, A., Bohr, T., Hansen, J. L. & Watanabe, S. 1999 Polygonal hydraulic jumps. *Nonlinearity* **12**, 1–7.

Ferro Fontan, C., Gratton, J. & Gratton, R. 1977 Self-similar implosion of shells. *Nucl. Fusion* **17**, 135–137.

Glendinning, P. 1994 *Stability, Instability and Chaos: An Introduction to the Theory of Nonlinear Differential Equations*. Cambridge University Press.

Gratton, J. 1991 Similarity and self similarity in fluid dynamics. *Fundam. Cosmic Phys.* **15**, 1–106.

Gratton, J. & Minotti, F. 1990 Self-similar viscous gravity currents: phase-plane formalism. *J. Fluid Mech.* **210**, 155–182.

Gratton, J. & Vigo, C. 1994 Self-similar gravity currents with variable inflow revisited: plane currents. *J. Fluid Mech.* **258**, 77–104.

Grigoryan, S. S. & Babkin, Y. V. 1998 Self-similar solution to equations describing shallow flows in large-scale water areas. *Dokl. Phys.* **43** (6), 373–377.

Gröbelbauer, H. P., Fanneløp, T. K. & Britter, R. E. 1993 The propagation of intrusion fronts of high density ratios. *J. Fluid Mech.* **250**, 669–687.

Grundy, R. E. & Rottman, J. W. 1986 Self-similar solutions of the shallow-water equations representing gravity currents with variable inflow. *J. Fluid Mech.* **169**, 337–351.

Guderley, G. 1942 Starke kugelige und zylindrische Verdichtungsstöße in der Nähe des Kugelmittelpunktes bzw. der Zylinderachse. *Luftfahrtforschung* **19**, 302–312.

Hallworth, M. A., Huppert, H. E. & Ungarish, M. 2003 On inwardly propagating high-Reynolds-number axisymmetric gravity currents. *J. Fluid Mech.* **494**, 255–274.

Hunter, C. 1960 On the collapse of an empty cavity in water. *J. Fluid Mech.* **8**, 241–263.

Hunter, C. 1963 Similarity solutions for the flow into a cavity. *J. Fluid Mech.* **15**, 289–305.

HUPPERT, H. E. 2000 Geological fluid mechanics. In *Perspectives in Fluid Dynamics: A Collective Introduction to Current Research* (ed. G. K. Batchelor, H. K. Moffatt & M. G. Worster), pp. 447–506. Cambridge University Press.

HUPPERT, H. E. & SIMPSON, J. E. 1980 The slumping of gravity currents. *J. Fluid Mech.* **99**, 785–799.

JENSEN, O. E. 1994 Self-similar, surfactant-driven flows. *Phys. Fluids* **6**, 1084–1094.

VON KÁRMÁN, T. 1940 The engineer grapples with nonlinear problems. *B. Am. Math. Soc.* **46**, 615–683.

PENNEY, W. G. & THORNHILL, C. K. 1952 The dispersion, under gravity, of a column of fluid supported on a rigid horizontal plane. *Phil. Trans. R. Soc. Lond.* A **244**, 285–311.

SCHWENDEMAN, D. W. & WHITHAM, G. B. 1987 On converging shock waves. *Proc. R. Soc. Lond.* A **413**, 297–311.

SEDOV, L. I. 1959 *Similarity and Dimensional Methods in Mechanics*. Academic.

SHIN, J. O., DALZIEL, S. B. & LINDEN, P. F. 2004 Gravity currents produced by lock exchange. *J. Fluid Mech.* (to appear).

SIMPSON, J. E. 1997 *Gravity Currents: in the Environment and the Laboratory*. Cambridge University Press.

WATANABE, S., PUTKARADZE, V. & BOHR, T. 2003 Integral methods for shallow free-surface flows with separation. *J. Fluid Mech.* **480**, 233–265.

WHITHAM, G. B. 1956 A new approach to problems of shock dynamics. Part I: Two-dimensional problems. *J. Fluid Mech.* **2**, 145–171.

WHITHAM, G. B. 1974 *Linear and Nonlinear Waves*. Wiley.

YIH, C.-S. & GUHA, C. R. 1955 Hydraulic jumps in a fluid system of two layers. *Tellus* **7**, 358–366.